Kinetic Parameters for the Vesicular Acetylcholine Transporter: Two Protons Are Exchanged for One Acetylcholine†

Marie L. Nguyen, Gregory D. Cox, and Stanley M. Parsons*

Department of Chemistry, Program in Biochemistry and Molecular Biology, and Neuroscience Research Institute, University of California, Santa Barbara, California 93106

Received January 28, 1998; Revised Manuscript Received June 22, 1998

ABSTRACT: The vesicular acetylcholine transporter (VAChT) mediates ACh storage in synaptic vesicles by exchanging cytoplasmic ACh with vesicular protons. This study sought to determine the stoichiometry of exchange by analysis of ligand binding and transport kinetics. The effects of different pH values inside and outside, external ACh concentrations, and electrical potential gradients on ACh transport by vesicles isolated from the electric organ of *Torpedo* were determined using a pH-jump protocol. The equilibrium binding of a high-affinity analogue of ACh is inhibited by protonation with a pK_a of 7.4 ± 0.3. A two-proton model fits the transport data much better than a one-proton model does, and uptake increases at more positive internal electrical potential, as expected for the two-proton model. Thus, the results support the two-proton model. The transport cycle begins with binding of external ACh to outwardly oriented site 2 (K_{ACho} = 20 mM) and protonation of inwardly oriented site 1 (pK_{a1} = 4.73 ± 0.05). Loaded VAChT reorients quickly (73 000 min^{-1}) and releases ACh to the inside (K_{AChi} = 44 000 mM) and the proton to the outside. Unloaded, internally oriented site 2 binds a proton (pK_{a2} = 7.0), after which VAChT reorients (150 ± 20 min^{-1}) in the rate-limiting step and releases the proton to the outside to complete the cycle. Rate constants for the reverse direction also were estimated. Two protons provide a thermodynamic driving force beyond that utilized in vivo, which suggests that vesicular filling is regulated. Other phenomena related to VAChT, namely the time required to fill synaptic vesicles, the fractional orientation of the ACh binding site toward cytoplasm, orientational lifetimes, and the rate of nonquantal release of ACh from cholinergic nerve terminals, were computer-simulated, and the results are compared with physiological observations.

Storage of acetylcholine (ACh)[1] by synaptic vesicles is mediated by the vesicular ACh transporter (VAChT), which catalyzes exchange of internal vesicular (luminal) protons for cytoplasmic ACh (*1*). The protons are supplied in vivo by V-type ATPase, which acidifies the lumen of vesicles about 2 pH units (*1*). No other ions are required for ACh transport (*2*). The cytoplasmic concentration of ACh is 1−4 mM. The concentration of ACh in full vesicles is about 160−600 mM, depending on the species of animal (*1*, *3*). The compound (−)-*trans*-2-(4-phenylpiperidino)cyclohexanol, also called vesamicol, potently inhibits VAChT (*4*).

A kinetics model for VAChT that ignores the roles of protons has been developed (*5*). The Michaelis constant of 0.3 mM is about 100-fold lower than the ACh dissociation constant. The model specifies neither the number of protons exchanged per ACh nor the microscopic step(s) for proton binding and translocation.

The mechanistic roles of protons in VAChT function have not been studied. The pH must be varied on both sides of the membrane for such studies. But the internal pH is set by the V-type ATPase, and variation of external pH affects the activity of the V-type ATPase. Thus, a method for driving ACh transport independently of ATPase activity must be used to quantitatively study proton interactions with VAChT.

A "pH-jump" protocol for studying ACh transport that is independent of ATPase activity has been developed (*6*). Vesicles are hypoosmotically lysed at low pH. After they reseal, the pH of the suspension is raised rapidly. ACh transport occurs for about 5 min, after which it stops due to collapse of the proton gradient. The effect of different internal pH values on ACh transport was studied preliminarily. Transport of a subsaturating concentration of [^{3}H]ACh exhibits a maximum at an initial internal pH of ∼5.0 and decreases steeply to zero at higher and lower values.

† This research was supported by a grant from the Muscular Dystrophy Association and by Grant NS15047 from the National Institute of Neurological Disorders and Stroke.

* Address correspondence to this author. Telephone: (805) 893-2252. Fax: (805) 893-4120. E-mail: parsons@chem.ucsb.edu.

[1] Abbreviations: ACh, acetylcholine; ACh_i, concentration of inside free ACh (in millimolar); ACh_o, concentration of outside free ACh (in millimolar); analogue 16/17, (±)-*cis*,*trans*-1-benzyl-1-methyl-3-(benzoyloxy)pyrrolidinium iodide; EDTA, ethylenediaminetetraacetic acid; EGTA, ethylene glycol bis(β-aminoethyl ether)-*N*,*N*,*N*′,*N*′-tetraacetic acid; FCCP, *p*-trifluoromethoxyphenylhydrazone; HEPES, *N*-(2-hydroxyethyl)piperazine-*N*′-2-ethanesulfonic acid; pH_i, initial internal (luminal) pH; pH_o, outside (cytoplasmic) pH; VAChT, vesicular acetylcholine transporter; vesamicol, (−)-*trans*-2-(4-phenylpiperidino)-cyclohexanol; VMAT, vesicular monoamine transporter.

S0006-2960(98)00226-8 CCC: $15.00
Published on Web 09/05/1998

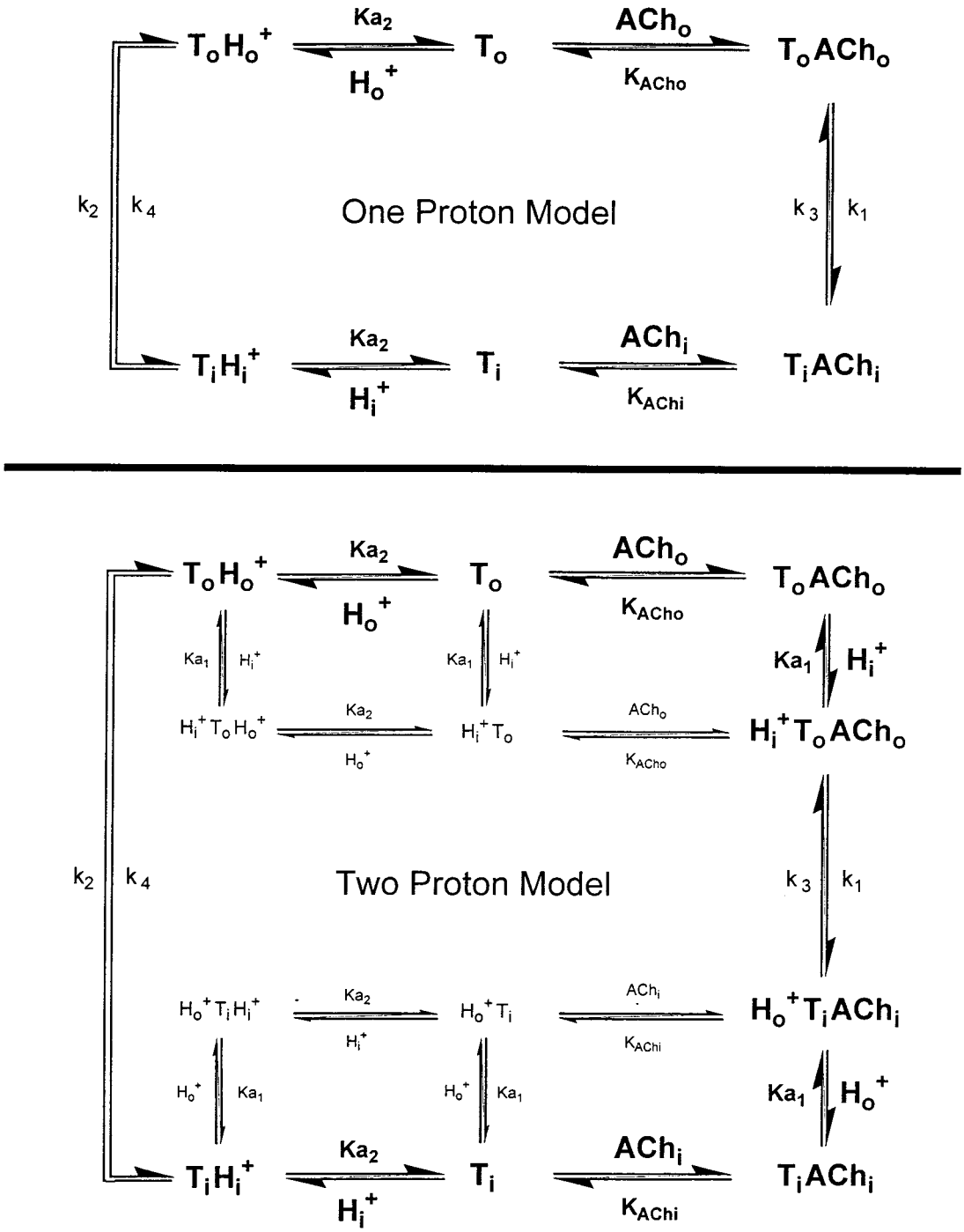

FIGURE 1: Possible kinetic mechanisms for VAChT in which protons are specified. Uptake of ACh occurs as the transporter cycles in a clockwise manner. ACh_o is the concentration of free ACh on the outside (cytoplasmic side) of the vesicle and ACh_i that on the inside (luminal side). T_o is unloaded transporter with its ACh binding site oriented toward the outside. T_oACh_o is the outwardly oriented transporter loaded with ACh; T_iACh_i is the inwardly oriented transporter loaded with ACh, and T_i is unloaded transporter with its ACh binding site oriented toward the inside. In the one-proton model, an internal proton (H_i^+) replaces ACh after it dissociates to the inside, and $T_iH_i^+$ is formed. This occurs at binding site 2 (pK_{a2}). $T_iH_i^+$ reorients across the membrane to form $T_oH_o^+$, which dissociates the translocated proton to the outside pool of protons (H_o^+). In the two-proton model, the same type of protonation event occurs, and in addition, an internal proton binds to T_oACh_o at protonation site 1 (pK_{a1}) to form $H_i^+T_oACh_o$. This species reorients across the membrane to form $H_o^+T_iACh_i$, which loses the translocated proton to the outside and ACh to the inside. Binding of protons and ACh can occur randomly to generate the other species in the figure. Binding of ACh is hypothesized to be at equilibrium outside and inside of the vesicle with dissociation constants K_{ACho} and K_{AChi}, respectively. Reorientation of the ACh binding site across the membrane in the "forward" direction occurs with rate constants k_1 and k_2. Reorientation in the "reverse" direction occurs with rate constants k_3 and k_4 and causes efflux of ACh.

In this study, the effects of pH, ACh concentration, and electrical potential gradients on ACh transport were examined in detail using the pH-jump method. The effect of pH on binding of a high-affinity analogue of ACh also was determined. A major goal of the work was to determine whether one or two protons are exchanged per ACh molecule. Possible models for the exchange are shown in Figure 1.

Because ACh transport was transient, standard steady state, Michaelis−Menten-like equations could not used to analyze

the data. Appropriate mathematical expressions were developed and fitted to the transport data. The optimized parameters from the fit and the other results allow a clear choice between the exchange models. The parameters also allow computer simulation of ACh transport characteristics in vivo, namely the filling time for vesicles, the fractional orientation of the ACh binding site toward cytoplasm, orientational lifetimes, and the rate of nonquantal leakage of ACh from nerve terminals.

EXPERIMENTAL PROCEDURES

Materials. VP_1 synaptic vesicles were isolated from the electric organ of *Torpedo californica* as described (*7*). The isolation involves homogenization of the tissue, differential sedimentation velocity pelleting onto a sucrose/Ficoll cushion, and equilibrium buoyant-density banding in sucrose. The final size exclusion chromatography step yields vesicles in 780 mM glycine, 5 mM HEPES, 1 mM EGTA, 1 mM EDTA, and 0.01% NaN_3 adjusted to pH 7.0 (with KOH, except for "sodium-isolated" vesicles for which NaOH was used throughout). Purified vesicles were concentrated to about 1 mg of protein per milliliter using Centricon centrifugal ultrafiltration devices (Amicon Corp.). Protein was quantitated as described (*8*) with bovine serum albumin as the standard. Vesamicol is available from Research Biochemicals, Inc. (Natick, MA). Liquid scintillation cocktail was made up to 3% in water to facilitate dissolution of [^{3}H]ACh. [^{3}H]ACh (74.8 mCi/mmol) and [^{14}C]methylamine hydrochloride (55 mCi/mmol) were from New England Nuclear. [^{14}C]Ribitol (55 mCi/mmol) was obtained from American Radiolabeled Chemicals Corp. [^{3}H]Analogue 16/17 [(±)-*cis*,*trans*-1-benzyl-1-methyl-3-(benzoyloxy)pyrrolidinium iodide] (49 mCi/mmol) was a gift from E. D. Clarkson, III. Other reagents were obtained from the usual commercial sources.

Transport and Binding. All operations were carried out at 23 °C. Vesicles were incubated with 200 μM diethyl-*p*-nitrophenyl phosphate (paraoxon) for 30 min to inhibit ACh esterase. Defatted bovine serum albumin was added to a final concentration of 1 mg/mL of vesicular suspension. Vesicles were lysed by the addition of a 4-fold volume of citrate buffer (100 mM $H_3C_6H_5O_7 \cdot H_2O$) adjusted to the desired pH with KOH (or NaOH as noted). The pHs quoted are the values after mixing. Lysed vesicles were incubated for 10 min. [^{3}H]ACh, [^{14}C]methylamine·HCl, [^{14}C]ribitol, [^{3}H]analogue 16/17, and vesamicol were deposited in a thin film dried from ethanol. Vesicles were added and allowed to incubate for 20 min. Two hundred millimolar HEPES-KOH (or NaOH as noted) at pH 13 and an additional amount of 200 mM HEPES-KOH (or NaOH as noted) at the target pH were added to give final concentrations of [^{3}H]ACh as indicated and vesicular protein at 0.075 mg/mL. Polyethylenimine-coated (0.5% for 3 h and then rinsed well in water) glass fiber filters (type GF/F, Whatman) were prewashed with ice-cold 200 mM HEPES-KOH (pH 7.8) using vacuum-assisted filtration. At indicated times, portions of the vesicular suspension (typically, 100−300 μL) were filtered. Unbound isotopes immediately were removed with three 1 mL washes of ice-cold buffer. Bound radioactivity was determined by liquid scintillation spectroscopy. Nonspecific binding of radioisotope was measured in 2 μM vesamicol. Disintegrations per minute for each isotope were determined as described (*9*). Specific transport or binding was calculated by subtracting the nonspecific binding determined by linear regression analysis from the total binding. Errors quoted are one standard deviation.

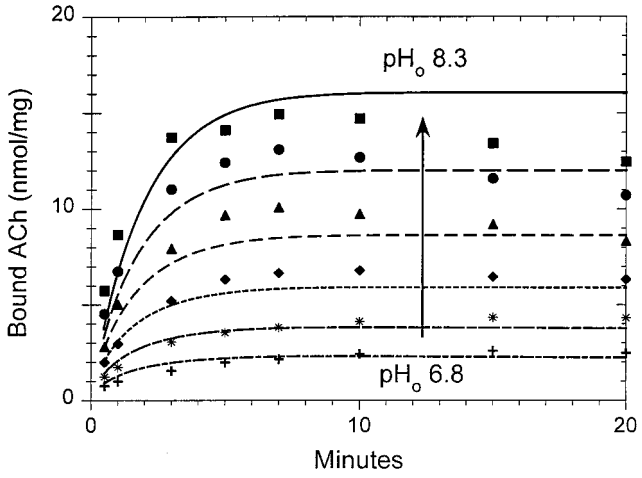

FIGURE 2: Time course of [^{3}H]ACh transport at different values of pH_o. Lysed vesicles at initial pH_i 5.1 were taken through the pH jump in 50 μM [^{3}H]ACh_o. The amounts of specific transport at different values of pH_o (6.8, +; 7.1, *; 7.4, ◆; 7.7, ▲; 8.0, ●; and 8.3, ■) at the indicated times after the pH jump are shown (this is the An1 data set in the regression). Similar results were obtained with three other preparations of vesicles.

Regression and Simulation Analyses. The software program Scientist (MicroMath Scientific Software, Salt Lake City, UT) was used to perform simultaneous regression to unweighted data in Figures 2−4 on a 150 MHz Pentium computer. Quoted errors are one standard deviation. Optimized parameters were used to perform simulations of other transport phenomena. The regression program and simulation expressions for the two-proton model are documented in the Appendix.

RESULTS

Resealing after Hypoosmotic Lysis at Different pH Values. Although essentially all lysed vesicles reseal right side out at pH 7.8 (*10*), the efficiency of resealing at other pH values is not known. This was determined as follows. Vesicles were lysed in [^{14}C]ribitol at pH values ranging from 4.3 to 8.1. Ribitol passes through the membrane nonspecifically and equilibrates at equal concentrations. The same amount of [^{14}C]ribitol was taken up from pH 5.2 to 8.1, and it corresponded to an internal volume of 6.0 μL/mg of protein (data not shown). This result is consistent with successful resealing of dispersed, monomeric vesicles. Below pH 5.0, the amount of trapped [^{14}C]ribitol increased substantially, suggesting fusion of vesicles. Thus, lysis below pH 5.0 cannot be used, and transport behavior below the initial pH of 5 was not analyzed.

Effects of pH_o on the Time Course of ACh Transport. Protons translocated by VAChT to the outside of the vesicle presumably are bound by specific amino acids before dissociating. Loading of these sites by external protons will inhibit ACh transport. To examine this, vesicles at the same initial inside pH (pH_i) were jumped to different outside pH values (pH_o) in the presence of outside [^{3}H]ACh. The amount of [^{3}H]ACh transported is shown in Figure 2. Transport was maximal at 5−7 min. Less transport occurred

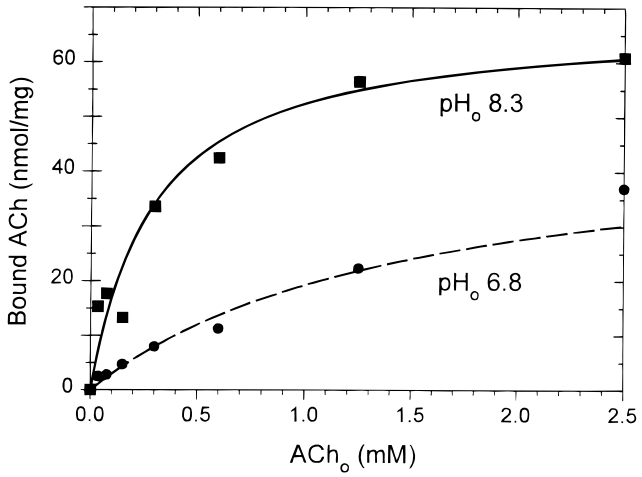

FIGURE 3: Transport at different [^{3}H]ACh$_o$ and pH$_o$ values. Lysed vesicles at an initial pH$_i$ of 5.1 were taken through the pH jump in the presence of the indicated concentrations of [^{3}H]ACh$_o$. The amounts of specific transport were determined at 7 min for pH$_o$ 6.8 (●) and pH$_o$ 8.3 (■) (this is the An2 data set in the regression). Similar results were obtained with one other preparation of vesicles.

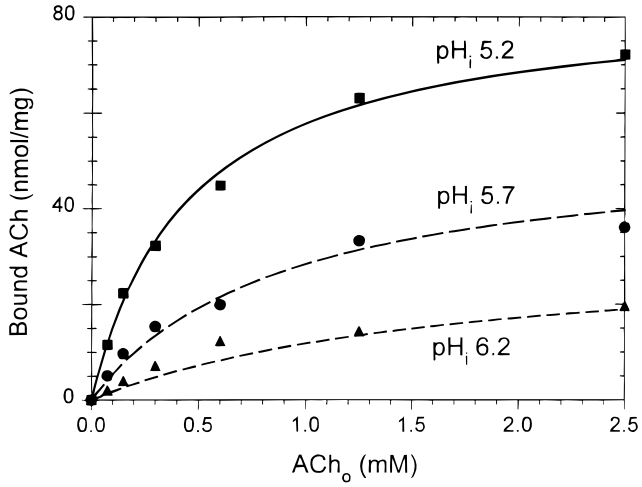

FIGURE 4: Transport at different [^{3}H]ACh$_o$ and pH$_i$ values. Lysed vesicles were taken through the pH jump in the presence of the indicated concentrations of [^{3}H]ACh$_o$. The amounts of specific transport were determined at 5 min at initial pH$_i$s of 5.2 (■), 5.7 (●), and 6.2 (▲) (this is the An3 data set in the regression). Similar results were obtained with one other preparation of vesicles.

at lower pH$_o$, suggesting that external protons are inhibitory. Inside [^{3}H]ACh slowly leaked out at higher pH$_o$, whereas it did not at lower pH$_o$.

Effects of pH$_o$ on Transport at Different Concentrations of Outside [^{3}H]ACh. Transport was titrated with outside [^{3}H]-ACh (ACh$_o$) at pH$_o$ 6.8 and 8.3 (Figure 3). At pH$_o$ 8.3, transport exhibited near saturation at 2.5 mM ACh$_o$. At pH$_o$ 6.8, less transport occurred, confirming that external protons are inhibitory.

Effects of pH$_i$ on Transport at Different Concentrations of Outside [^{3}H]ACh. Transport was titrated with [^{3}H]ACh$_o$ at initial pH$_i$ values of 5.2, 5.7, and 6.2 (Figure 4). At lower pH$_i$ values, more transport occurred, demonstrating that internal protons are stimulatory.

Regression Fit to Transport Data. The models in Figure 1 are consistent with the transport data. Mathematical expressions corresponding to them are developed in the Appendix. They include the mechanistic parameters shown in Figure 1 and extramechanistic parameters arising from phenomena not intrinsic to functional VAChT. The latter parameters are the rate of decay for the proton gradient (k_5) and the relative transport specific activities of vesicular preparations (*b* and *c*). The key equations are differentials in time, which are integrated numerically. The concentrations of internal protons and all forms of ACh and VAChT are computed as time increases. Strategies for reducing the number of adjustable parameters to obtain determinant regression are described in the Appendix overview.

Table 1: Results of Regression[a]

parameter	one-proton fit	two-proton fit
Σ (nmol^2/mg^2)	**898**	**447**
K_{ACho} (mM)	20	20
K_{AChi} (mM)	270 000	44 000
pK_{a1}	–	**4.73 ± 0.05**
pK_{a2}	7.0	7.0
k_1 (min^{-1})	26 000	73 000
k_2 (min^{-1})	**260 ± 90**	**150 ± 20**
k_3 (min^{-1})	10^{10}	10^{10}
k_4 (min^{-1})	**9.4 ± 1.9**	**2.3 ± 0.7**
k_5 (min^{-1})	**0.29 ± 0.03**	**0.78 ± 0.11**
b	**0.69 ± 0.04**	**0.63 ± 0.04**
c	**0.98 ± 0.06**	**0.91 ± 0.06**

[a] The standard preparation of vesicles (Figure 2) was assumed to have 240 pmol of functional VAChT per milligram of protein. Values for the parameters in regular type were assumed or computed as described in the Appendix. Adjustable parameters estimated by the regression program are bold and quoted to two significant figures. Σ is the sum of the squares of the errors. Rate constants are for individual molecules of VAChT. Parameters *b* and *c* give the ratios of the specific transport activities of the vesicles used in Figures 3 and 4 compared to those used in Figure 2. The *F* test and the likelihood ratio test demonstrate that the two-proton model is very much preferred [$F_{(1,79)} = 40$ ($p \ll 0.001$); $C_{(1,85)} = 26$ ($p \ll 0.005$)]. Exclusion of the data in Figure 2 that deviated the most from the regressions (at pH$_o$ 8.3 and 8.0) did not change the *p* values significantly. Parameters for the two-proton model were used to draw the lines shown in Figures 2−4.

The remaining adjustable parameters were optimized by a simultaneous fit to the data in Figures 2−4. Similar results were obtained starting with different initial estimates. Optimized values for the one- and two-proton models are given in Table 1. The best-fit lines for the two-proton model are shown (Figures 2−4). The fit is excellent, except to the data exhibiting leakage of inside [^{3}H]ACh at high pH$_o$ in Figure 2. Leakage was a variable phenomenon that did not occur in every preparation of vesicles, and thus probably arises from some feature of the transporter not modeled here.

The estimates for corresponding parameters in the models are similar (Table 1). We first present the mechanistic parameters. The K_{AChi} estimates are large compared to K_{ACho}, being 270 000 and 44 000 mM compared to 20 mM for the one- and two-proton models, respectively. However, because it is strongly correlated with k_3, which was capped at the highest possible value (see the Appendix), K_{AChi} is not well determined. The best conclusion is that k_3 and K_{AChi} are very large relative to the other rate and equilibrium constants. Thus, vesicular ACh binds very weakly to inwardly oriented VAChT. The estimated values for k_1 are 26 000 and 73 000 min^{-1} for the two models. No error is given because k_1 is computed from k_2 (see the Appendix). Estimated values of k_2 are 260 ± 90 and 150 ± 20 min^{-1}. The k_2 rate constant is well determined because it is rate-limiting in the ACh uptake cycle. The estimated values of k_4 are the smallest of

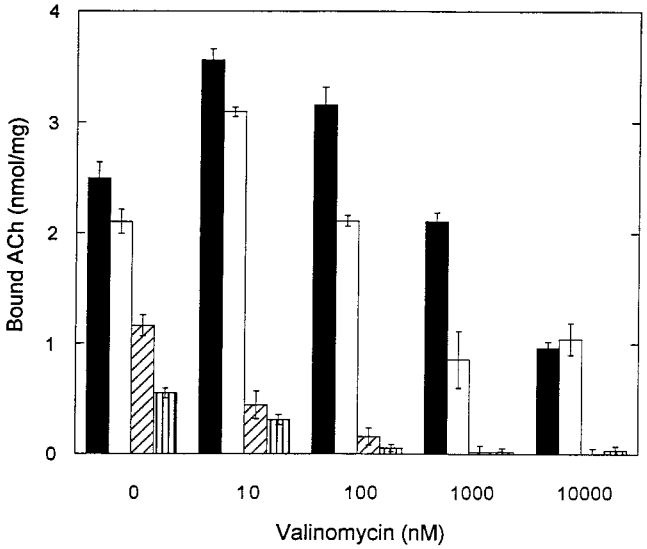

FIGURE 5: Effects of FCCP and valinomycin on ACh transport. Lysed vesicles were taken through the pH jump from 5.1 to 7.8 in the presence of 50 μM [^{3}H]ACh$_o$ and FCCP (0, filled; 10 nM, empty; 100 nM, diagonally hatched; and 1 mM, vertically hatched) at the indicated concentrations of valinomycin. The amount of specific transport 5 min after the pH jump is shown as the mean of triplicates. Similar results were obtained with one other preparation of vesicles.

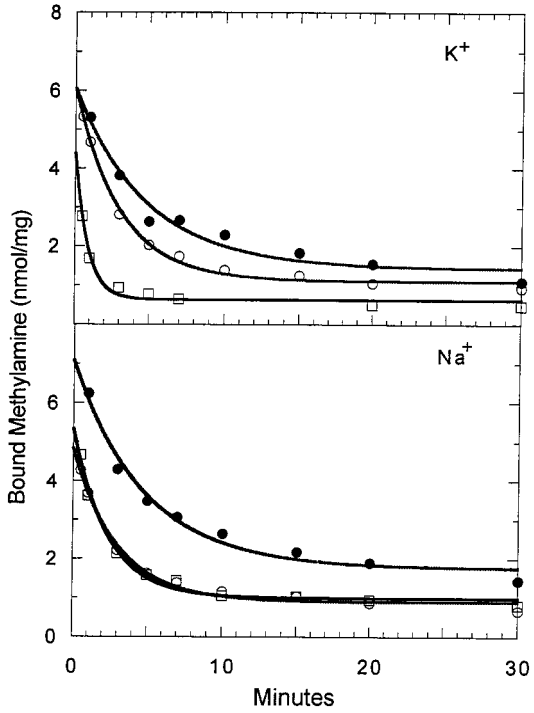

FIGURE 6: Effect of a more positive internal electrical potential on proton efflux after the pH jump. Na^+-isolated vesicles were subjected to hypoosmotic lysis in the presence of 2 μM [^{14}C]-methylamine and 50 μM [^{3}H]ACh$_o$ at pH$_o$ 5.1 in the presence of no other additions (○) or sufficient reagents to yield final concentrations of 100 nM valinomycin (□) or 2 μM vesamicol (●). The pH$_o$ was jumped to 7.8 with 0.20 M HEPES adjusted to alkaline pH with either KOH or NaOH. The top and bottom frames show the amounts of [^{14}C]methylamine bound in the presence of external K^+ and Na^+, respectively, as determined by liquid scintillation spectroscopy in the double-channel mode. Rate constants for the loss of [^{14}C]methylamine and thus protons obtained by regression analysis are listed in Table 2. Similar results were obtained with one other preparation of vesicles.

the rate constants, being 9.4 ± 1.9 and 2.3 ± 0.7 min^{-1}. This means that ACh-free VAChT effectively cannot reorient from the cytoplasm to the inside of the vesicle. Finally, the protonation site common to both models has a pK_{a2} of 7.0, and the additional protonation site in the two-proton model has an estimated pK_{a1} of 4.73 ± 0.05.

We next present the extramechanistic parameters. The estimated values of k_5 for decay of the proton gradient are 0.29 ± 0.03 and 0.78 ± 0.11 min^{-1}. Estimated ratios of transport specific activity for the vesicles used in Figure 3 compared to those used in Figure 2 were 0.69 ± 0.04 and 0.63 ± 0.04 for the two models. The ratios for the vesicles used in Figure 4 compared to those used in Figure 2 were 0.98 ± 0.06 and 0.91 ± 0.06.

Introduction of pK_{a1} in the two-proton model increases the number of adjustable parameters from five to six. This decreased the sum of the squares of the errors from 898 to 447 nmol^2/mg^2. The decrease is very significant and indicates that the two-proton model is strongly preferred ($p \ll 0.001$ and $p \ll 0.005$ by the F and likelihood ratio tests, respectively).

Effects of a More Positive Transmembrane Electrical Potential on ACh Transport. A 2:1 exchange stoichiometry suggests that more positive internal electrical potential will stimulate ACh uptake. This was tested. Synaptic vesicles in K^+-containing buffer exposed to nothing else or to varying concentrations of the protonophore carbonyl cyanide *p*-trifluoromethoxyphenylhydrazone (FCCP) and the K^+ ionophore valinomycin were taken through the pH jump (Figure 5). As expected, concentrations of ≥100 nM for FCCP inhibited transport and concentrations of ≥100 nM for valinomycin potentiated the inhibition (*2*). However, at 0 and 10 nM FCCP, 10 nM valinomycin stimulated transport by as much as 40%. Higher concentrations of valinomycin inhibited transport, probably because of nonspecific disruption of the membrane. This result indicates that a more positive internal electrical potential increases uptake of ACh under some conditions, suggesting that transport occurs with net efflux of positive charge.

The effects of electrical potential on ACh transport were investigated further. Vesicles were lysed in Na^+ buffer with [^{3}H]ACh and [^{14}C]methylamine in the absence or presence of minimally effective valinomycin. No FCCP was present. The external pH then was jumped with K^+- or Na^+-containing buffer. Methylamine accumulates in acidic compartments and accurately reflects collapse of the transmembrane proton gradient (*6*).

The amounts of [^{14}C]methylamine and [^{3}H]ACh taken up by vesicles at different times after the pH jump are shown in Figures 6 and 7, respectively. Rate constants for proton efflux are given in Table 2. With external K^+, valinomycin induced a 3.5-fold more rapid collapse of the proton gradient, demonstrating that the vesicles indeed became more positive inside. With external Na^+, valinomycin induced only a small increase in the rate of proton efflux (Table 2). The faster rate of proton loss had no significant effect on the total amount of [^{3}H]ACh taken up (Figure 7). The more positively charged vesicles apparently transported ACh faster for a shorter period. The result demonstrates that a positive internal potential substituted for internal protons, implying that ACh uptake occurs with net efflux of positive charge.

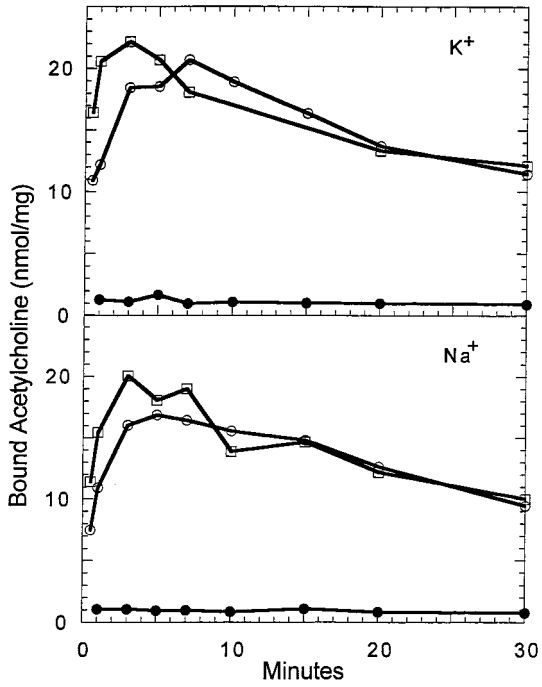

FIGURE 7: Effect of a more positive internal electrical potential on [^{3}H]ACh transport. These data came from the other scintillation channel in the same experiment depicted in Figure 6. The top and bottom frames show the results in external K^+ and Na^+, respectively. Similar results were obtained with one other preparation of vesicles.

Table 2: Rate Constants for Proton Efflux Addition[a]

addition[a]	rate constant (min^{-1})	
	K^+-based buffer	Na^+-based buffer
none	0.33 ± 0.03	0.33 ± 0.03
valinomycin (100 nM)	1.2 ± 0.3	0.42 ± 0.05
vesamicol (2 μM)	0.33 ± 0.03	0.21 ± 0.03

[a] Regression values obtained from exponential fits of the data in Figure 6.

Effect of pH on Binding of ACh Analogue 16/17. This analogue binds tightly enough to allow observation of equilibrium binding in the absence of transport (*11*). Equilibrium binding of ACh itself cannot be observed directly with available assays because it is too weak. In the absence of any pH gradient, binding increased from a very small amount at low pH to a maximal amount at high pH with a pK_a value of 7.4 ± 0.3 (Figure 8). A proton having this pK_a probably also inhibits binding of ACh.

DISCUSSION

Conflicting information regarding the likely exchange stoichiometry exists. The proton and ACh gradients in vivo are about 100-fold (*1*). This is equilibrium in a one-to-one exchange. The vesicular monoamine transporter (VMAT) exchanges two protons for each monoamine (*12*). VAChT and VMAT are homologous (*13*, *14*), which suggests similar mechanisms of transport.

Determination of ACh, proton, and electrical potential gradients at equilibrium would give the stoichiometry of exchange (*15*). However, we have not been able to establish equilibrium gradients. Instead, we approached the stoichiometry by developing a pH-jump protocol to drive transport.

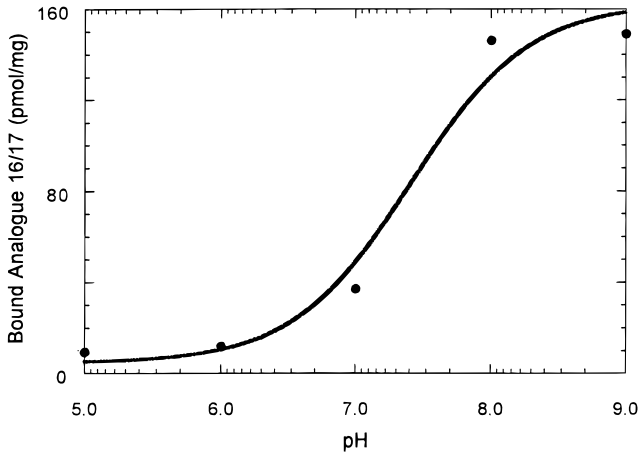

FIGURE 8: Binding of subsaturating [^{3}H]analogue 16/17 concentrations at different pH values. Lysed vesicles were adjusted to the indicated pH values and incubated for 15 min to allow decay of any pH gradient before addition of 500 nM [^{3}H]analogue 16/17. Binding was measured in triplicate after further incubation for 30 min. A rectangular hyperbola was fit to the averaged specific binding data, which exhibited a standard deviation of less than 5%, as a function of the proton concentration to estimate a pK_a value of 7.4 ± 0.3.

Quantitative analysis required development of the mathematical expressions described in the Appendix. The method extracts rate and dissociation constants from the data, which is not possible in equilibrium measurements.

Data Modeling. Simultaneous regression to the data in Figures 2−4 yielded determinant values for adjustable parameters when constraints described in the Appendix were applied. We justify a parameter for relative specific activity of transport because some vesicular preparations (not used for these experiments) did not transport well. The rate constant for decay of the proton gradient was similar to values determined in Table 2 and elsewhere (*6*).

A pK_a of 7.1 has been measured to good accuracy by competition against binding of [^{3}H]vesamicol (J. E. Keller and S. M. Parsons unpublished results). Titration in the pH-jump buffer yielded a pK_a of 7.0 (M. L. Nguyen, unpublished observation). We assign this protonation to the transport site because (1) a pK_a of 7.4 ± 0.3 controls binding of an ACh analogue and (2) ACh and vesamicol bind to overlapping sites (J. E. Keller and S. M. Parsons unpublished observation). Protonation was placed at the k_2-k_4 reorientation step (binding site "2"), because that creates a reciprocating pump. The pK_a value is consistent with histidine, which likely is conserved because of its role in binding ACh and a proton. Histidine residue 323 (in putative transmembrane domain 8) of *Torpedo* VAChT (*16*) is the only conserved histidine.

VAChT Exchanges Two Protons per ACh. Placement of a second translocated proton at the k_1-k_3 reorientation step (binding site "1") greatly improved the fit. This was true for all fit variations tried, such as using additional adjustable parameters and data weighting. The estimated pK_{a1} value of 4.73 ± 0.05 is consistent with an aspartate or glutamate residue. Four aspartates are absolutely conserved in VAChT and VMAT (*13*), and two of them (in putative transmembrane domains 4 and 10) have been shown to be essential for ACh transport (*17*).

The electrical potential gradient in cholinergic vesicles never has been measured reliably. Hypoosmotic lysis of

similar vesicles creates small transient pores that do not allow loading with controlled concentrations of K^+ (*18*), making it difficult to clamp intravesicular electrical potential at a known value. Nevertheless, unknown electrical potential has no effect on the regression analysis. Because it fits the data much better and ACh transport occurs with net efflux of positive charge, the two-proton model is preferred.

Kinetic and Thermodynamic Characteristics of VAChT. The k_1-k_3 reorientation step is relatively rapid in both directions, which is consistent with a channel-like VAChT (*5*). The relative slowness of the k_2-k_4 reorientation step might be related to different electrical loadings.

In the previous model (*5*), the k_2 estimate was 5.4 min^{-1} in the best preparation of synaptic vesicles studied, which is much less than the 150 min^{-1} estimate in this work. The earlier estimate did not account for the pH dependence of transport. Also, many vesicles did not transport, as much of the fragile V-type ATPase is damaged during purification.

Because it is rate-limiting, k_2 is similar to the turnover rate V_{max}/B_{max}. The k_2 value determined here is close to the V_{max}/B_{max} value of 65 min^{-1} determined by Varoqui and Erickson (*19*) for human VAChT expressed in PC12 cells. The affinities for vesamicol are nearly the same in the two species. Thus, *Torpedo* and human VAChTs are similar functionally.

A 100-fold proton gradient provides an electrochemical driving force theoretically sufficient to establish a greater than 10^4-fold gradient of ACh, which is much greater than the gradient in vivo. This implies that VAChT is regulated. Evidence for regulation has been reported. Vesamicol binding and ACh transport by *Torpedo* vesicles are related reciprocally (*7*, *20*). Phosphorylation blocks inhibition of transport by vesamicol in brain and myenteric plexus (*21*, *22*). The size of the quantum (ACh per vesicle) released from motor terminals can be increased 3-fold by manipulation of second messengers (*23*, *24*). Also, overexpression of VAChT in developing *Xenopus* spinal neurons increases quantal size up to 10-fold (*17*).

Simulation of Physiological Observations. With k_5 set to zero, the parameters in Table 1 allow computer simulation of ACh fluxes in vivo. Neglecting electrical potential will produce error, but the free energy in a realistic electrical gradient of about 50 mV is small compared to that in the square of the proton gradient. Thus, these simulations likely will not produce conceptual error. Simulations of this sort have not been done before, and they raise new issues that should be addressed in the function of vesicular transporters.

The time course for filling of *Torpedo* vesicles with the two-proton model is simulated in Figure 9. It takes about 1000 min to reach 600 mM ACh_i, which is physiologically full (*3*). It takes about 850 000 min to reach 95% of the thermodynamically full value of 10 000 mM. The physical impossibility of attaining the equilibrium concentration, which is greater than that of an anhydrous salt of ACh, does not invalidate the model for lower ACh_i.

Because the kinetics of *Torpedo* and human VAChTs are similar, we can apply the simulation to vesicles from higher vertebrates. The volume of the lumen in such vesicles is about 10-fold smaller than that in electric organ vesicles, and ACh_i is only about 160 mM (*3*). A *Torpedo* vesicle takes about 90 min to pump 160 mM ACh_i (Figure 9). A human vesicle containing as many VAChTs would take about

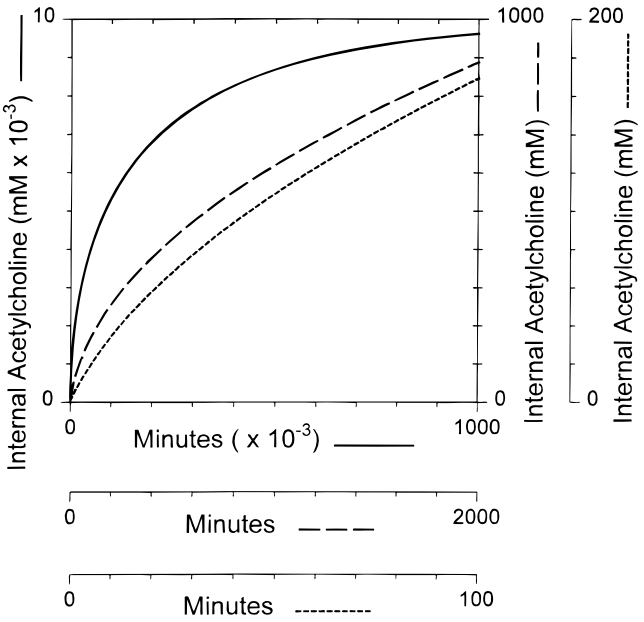

FIGURE 9: Computer-simulated filling of a *Torpedo* synaptic vesicle by the two-proton model of transport. ACh_i is plotted vs time on three scales starting with an empty *Torpedo* synaptic vesicle. The two-proton parameters of Table 1 were used for the simulation, except that k_5 (the rate of decay of the driving force for uptake) was set at 0. The independent variables ACh_o, pH_o, and pH_i were set to 1 mM, 7.3, and 5.3, respectively. The model correctly simulates uptake of 10^4 mM ACh_i at equilibrium.

9 min. This should be compared with the estimated 1−2 min required for recycling of previously released vesicles (*24*). Clearly, vesicles must refill in less than the recycling time, so there is apparent error in our estimated filling time. However, there are uncertainties in the number of VAChTs per vesicle, ACh_o, ACh_i, and values of the proton and electrical gradients in vivo. The uncertainties are great enough to allow physiological filling by the two-proton model in 1 min.

Because one-to-one exchange at equilibrium might just account for the amount of ACh stored in vivo, simulation of the filling time for the one-proton model is informative. Reaching 95% of equilibrium requires 1700 min in *Torpedo* vesicles and thus 170 min in the vesicles of higher vertebrates. These times are 19-fold longer than those required to reach 160 mM ACh_i in the two-proton model. Approach-to-equilibrium filling occurs asymptotically with inherent slowness which by itself suggests that vesicular and cytoplasmic ACh cannot reach equilibrium in the allowed time.

The simulations assume that vesicles refill in vivo as individuals. Recycling vesicles might be processed by intraterminal cisternae (*26*, *27*). The possibility that vesicles gain most of their ACh_i from cisternae should be considered. However, solid geometry does not support this in an active terminal. The ratio of surface area to volume for cisternae is smaller than that for vesicles. A longer time would be required to fill cisternae to 160 mM ACh_i, thus yielding no advantage over filling of individual vesicles.

The orientational behavior of the transporter in the two-proton model was simulated (Figure 10). Nearly empty (but transporting) vesicles have the ACh binding site mostly inwardly oriented. Outward orientation increases almost 5-fold as filling proceeds. The lifetime of the ACh binding

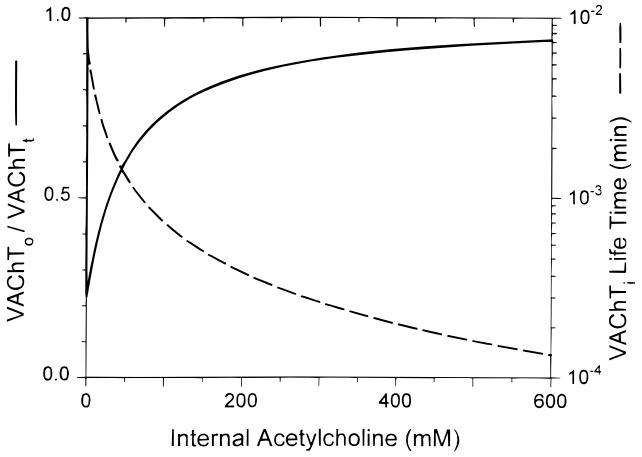

FIGURE 10: Computer-simulated fractional exposure of the ACh binding site to cytoplasm and lifetime τ_2 of inwardly oriented ACh binding site as vesicles fill with ACh. The parameters and independent variables of Figure 9 were used for the simulation. The ratio of the sum of the concentrations of all forms of outwardly oriented transporter divided by the total concentration of transporter ($VAChT_o/VAChT_t$) is plotted vs ACh_i during filling of a vesicle. In empty vesicles, the ACh binding site is exposed to cytoplasm 22% of the time. At 600 mM ACh_i, it is exposed 94% of the time. In thermodynamically full vesicles, it is exposed more than 99% of the time. The filling calculation assumed that all of the transporter is outwardly oriented at the beginning, but the time course after the initial transient of 0.015 min (when ACh_i is less than 0.1 mM) is not affected by the initial orientation. Also, the $VAChT_i$LifeTime (τ_2) is plotted vs ACh_i during filling of a vesicle (see eqs 19 and 20 in the Appendix). The cytoplasmic lifetime τ_1 is 0.0020 min and does not change with filling. The luminal lifetime τ_2 is 0.0070 min in an empty vesicle and 0.00013 min at 600 mM ACh_i. It is 8.2×10^{-6} min in a thermodynamically full vesicle.

site in the cytoplasmic (τ_1) and luminal (τ_2) orientations also was simulated (Figure 10). The τ_1 lifetime does not change during filling. Nearly empty (but transporting) vesicles exhibit a relatively long τ_2. As vesicles fill, τ_2 decreases due to activation of the k_3 step. In physiologically full vesicles, the decrease in τ_2 is more than 10-fold larger than the increase in cytoplasmic exposure of the ACh binding site.

The simulations suggest two possible mechanisms by which vesicles could sense satiety so they could shut off transport. The increase in exposure of the ACh binding site could be sensed from the cytoplasm, where regulatory mechanisms are plentiful. The larger decrease in τ_2 would have to be sensed from the vesicular lumen, where no known regulatory mechanism exists.

The equilibrium orientation of VAChT could affect apparent dissociation constants measured for ligands. Simulation with the two-proton model demonstrates that the ACh binding site is greater than 98% outwardly oriented from pH 5 to 8 (no pH gradient) for any combination of ACh_o and ACh_i up to 1000 mM. Thus, the 20 mM value taken for K_{ACho} in the regression is close to the true value and not perturbed by an adverse VAChT orientation.

Inactive cholinergic terminals release ACh in large excess (about 0.1 fmol per minute per terminal) over apparent quantal release (*28*, *29*). This nonquantal ACh might leak from cytoplasm through VAChT in the plasma membrane. Such leakage was simulated with the two-proton model ($pH_i = 7.3$ and $ACh_i = 10^{-12}$ mM), with the result being that each VAChT releases 5.5 molecules of ACh per minute. About 10^7 VAChTs would have to be in the plasma membrane to account for nonquantal release. As only about 10^5 vesicles are in a nerve terminal (*1*), and most VAChT is in the vesicles, nonquantal release probably occurs by a different mechanism.

Comparison to VMAT. The transport cycle and turnover rate of about 30 min^{-1} for VMAT (*12*) are similar to those proposed here for VAChT. Other features are different. In the absence of a pH gradient, VMAT orients away from the cytoplasm (*12*). Aminergic vesicles establish a greater than 10^4-fold concentration gradient, indicating that cytoplasmic and vesicular monoamines reach equilibrium (*13*). This is possible because monoamines are present at only low micromolar cytoplasmic concentrations. In summary, the basic transport mechanisms of VMAT and VAChT are similar, but VAChT has a regulatory overlay.

APPENDIX

Regression Analysis of ACh Transport after pH Jump

Overview. Regression is to experimental data composed of the dependent variables bound nanomoles of [^{3}H]ACh per milligram of vesicular protein (An1, An2, and An3) as a function of the independent variables time (t) after the pH jump, pH_o, pH_i, and ACh_o. pH_o and ACh_o do not change with time, whereas pH_i and ACh_i do.

The values of the mechanistic parameters k_1, k_3, pK_{a1}, pK_{a2}, K_{ACho}, and K_{AChi} were constrained or obtained as follows.

(a) Conjugate bases that bind and release a particular proton on different sides of the membrane could have different pK_a values if (1) they are a single base that reorients to a different environment or (2) they are different bases. Because this creates too many adjustable parameters, pK_a values for a particular proton were assumed to be the same on both sides of the membrane.

(b) pK_{a2} was fixed at 7.0 for the reason described in the Results.

(c) When point a is true, pK_a values cancel out in the thermodynamic cycle, and only five of the six remaining constants are independent. Thus, $K_{AChi} = K_{ACho}k_3k_4/(k_1k_2)$.

(d) In early analyses, k_3 was allowed to vary, but regression increased it to physically unrealistic values. As long as k_3 was large, the residuals and the values of the other parameters were hardly affected except for K_{AChi}, which increased in nearly direct proportion to k_3. This is because K_{AChi} and k_3 have opposing mechanistic effects and are linked by the thermodynamic cycle. Thus, k_3 was fixed at 10^{10} min^{-1}, the maximal value for ion channels (*30*) and surely faster than any transporter.

(e) The parameter k_1 was computed from k_2. In the one-proton model, the apparent ratio k_1/k_2 is 100 (*5*), and it essentially is equal to the true ratio under prevailing conditions. In the two-proton model, the apparent ratio is less than the true ratio due to only partial protonation of site 1. Thus k_1/k_2 was set to 500, as justified below.

(f) K_{ACho} was fixed at 20 mM, which is the lower limit of the consensus range of apparent values (*5*). This number allows for some increase in the apparent value due to competition by protons.

The remaining mechanistic parameters k_2, k_4, and pK_{a1} and the extramechanistic parameters k_5, b, and c were optimized

by the regression program for the two-proton model. pK_{a1} does not exist in the one-proton model. Computed variables and parameters not automatically reported, such as ACh_i, k_1, K_{AChi}, and VAChT$_i$LifeTime were listed as dependent variables so that the program would report and graph them.

Derivation of the Equations for the Two-Proton Model. The expressions for the one-proton model are a subset of those derived here. The pH and pK values first are converted to molarities using their definition. Protons are shown without their charges in equations. Thus, $K_{a1} = 10^{-\ pK_{a1}}$; $K_{a2} = 10^{-pK_{a2}}$, and $H_o = 10^{-pH_o}$. To compute H_i, we assume a first-order decay to H_o with rate constant k_5. Thus, $H_i = (10^{-pH_i} - H_o)e^{-k_5 t} + H_o$. The derivation is more compact if we normalize the concentrations of protons and ACh by dividing by the respective dissociation constants to compute the reduced concentrations of the ligands. For proton site 1, $H_o r1 = H_o/K_{a1}$ and $H_i r1 = H_i/K_{a1}$, and for site 2, $H_o r2 = H_o/K_{a2}$ and $H_i r2 = H_i/K_{a2}$. Also $ACh_o r = ACh_o/K_{ACho}$, and $ACh_i r = ACh_i/K_{AChi}$. $H_o r1$ stands for proton concentration outside reduced for site 1, and the full names of the other symbols can be deduced similarly.

We assume that the species in the top half of the two-proton panel in Figure 1 are in equilibrium with each other to form composite 1, and the species in the bottom half are in equilibrium with each other to form composite 2 (*31*). The rate of the reaction $H_i{}^+T_oACh_o \rightarrow H_o{}^+T_iACh_i$ is equal to $k_1[H_i{}^+T_oACh_o]$. As $H_i{}^+T_oACh_o$ is in equilibrium with the other species in composite 1, its concentration will be given by a fraction of composite 1 equal to

$$W = [1 + H_i r1^{-1} + ACh_o r^{-1} + (H_i r1 \times ACh_o r)^{-1} + H_o r2/(H_i r1 \times ACh_o r) + H_o r2/ACh_o r]^{-1} \quad (1)$$

The rate of transmembrane reaction of $H_i{}^+T_oACh_o$ then is given by

$$W_{Cr} = k_1 W[\text{composite 1}] \quad (2)$$

Similarly, the fraction of composite 2 that is $H_o{}^+T_iACh_i$ is equal to

$$X = [1 + H_o r1^{-1} + ACh_i r^{-1} + (H_o r1 \times ACh_i r)^{-1} + H_i r2/(H_o r1 \times ACh_i r) + H_i r2/ACh_i r]^{-1} \quad (3)$$

and the rate of transmembrane reaction of $H_o{}^+T_iACh_i$ is given by

$$X_{Cr} = k_3 X[\text{composite 2}] \quad (4)$$

where the concentration of composite 2 is given by

$$[\text{composite 2}] = [\text{VAChT}] - [\text{composite 1}] \quad (5)$$

and [VAChT] is the total concentration of active VAChT. For $T_iH_i{}^+$,

$$Y = [1 + H_o r1 + H_i r2^{-1} + H_o r1/H_i r2 + ACh_i r/H_i r2 + H_o r1 \times ACh_i r/H_i r2]^{-1} \quad (6)$$

and

$$Y_{Cr} = k_2 Y[\text{composite 2}] \quad (7)$$

and for $T_oH_o{}^+$,

$$Z = [1 + H_i r1 + H_o r2^{-1} + H_i r1/H_o r2 + ACh_o r/H_o r2 + H_i r1 \times ACh_o r/H_o r2]^{-1} \quad (8)$$

and

$$Z_{Cr} = k_4 Z[\text{composite 1}] \quad (9)$$

The rate of change in the concentration of composite 2 due to the k_1-k_3 reorientation step is the difference between the forward and backward rates through that step, or

$$d[\text{composite 2}]_{1-3}/dt = W_{Cr} - X_{Cr} \quad (10)$$

The rate of change in the concentration of composite 1 due to the k_2-k_4 reorientation step similarly is

$$d[\text{composite 1}]_{2-4}/dt = Y_{Cr} - Z_{Cr} \quad (11)$$

The net rate of formation of composite 1 is the difference between the rates toward and away from it through the two reorientation steps and is given by

$$d[\text{composite 1}]/dt = d[\text{composite 1}]_{2-4}/dt - d[\text{composite 2}]_{1-3}/dt \quad (12)$$

The above expressions are used to compute concentrations averaged over the solution.

The total amount of transported ACh at a particular time is given by the integral of eq 10 from 0 to t, or $ACh_t = [\text{composite 2}]_{1-3} = \int (W_{Cr} - X_{Cr})\, dt$. The species ACh_t will become concentrated because it is confined inside of the vesicles. The concentration ratio is given by the ratio of the solution to luminal volumes. However, not all of the ACh_t is released as ACh_i, because some remains bound to the transporter on the inside. ACh bound on the outside will not be assayed because it is bound too weakly. The fraction of composite 2 that is bound to the species ACh_t is given by

$$XX = (1 + H_o r1^{-1})X \quad (13)$$

and the rate of change in ACh_i is given by

$$dACh_i/dt = (0.04\ \text{mM}/[\text{VAChT}]) \times (d[\text{composite 2}]_{1-3}/dt - XX\ d[\text{composite 2}]/dt) \quad (14)$$

where 0.04 mM is the concentration of VAChT in the vesicular phase (estimated for a typical vesicular preparation containing 240 pmol of VAChT/mg of vesicular protein and 6.0 μL of lumen/mg of vesicular protein) and [VAChT] is averaged over the solution. In this work, [VAChT] was taken to be 1.8×10^{-5} mM for the An1 data set.

The vesicles that yielded An1 data in Figure 2 were considered "standard". The amount of transported ACh must be expressed in the units used for the data, so

$$An1 = ACh_t/[SV] \quad (15)$$

where [SV] is in milligrams of vesicular protein per microliter of total solution. In this work, [SV] was 7.5×10^{-5} mg/μL. An2 data in Figure 3 are related to An1 data by the ratio b of the specific transport activities for the vesicular preparations, or

$$\mathrm{An2} = b\mathrm{An1} \quad (16)$$

and An3 data in Figure 4 similarly are related to An1 data by

$$\mathrm{An3} = c\mathrm{An1} \quad (17)$$

The fraction of the ACh binding site in the outward orientation is

$$\mathrm{VAChT_o/VAChT_t} = [\text{composite 1}]/[\mathrm{VAChT}] \quad (18)$$

The lifetime of composite 1 is given by the reciprocal of the sum of the effective rate constants converting it to composite 2, or

$$\tau_1 = 1/(Wk_1 + Zk_4) \quad (19)$$

and the lifetime of composite 2 is given analogously by

$$\tau_2 = 1/(Xk_3 + Yk_2) \quad (20)$$

Additional Information That Is Available for Constraining the Ratio k_1/k_2. Previous work established that the apparent ratio of k_1/k_2 is about 100 when ACh transport is driven by ATP under steady state initial velocity conditions at pH_o 7.8 (*5*). The apparent ratio is not the true ratio because the transporter must be protonated before it can reorient. The rates of reorientation must be the same in the proton-independent model of Bahr et al. (*5*) and the proton-dependent model. Thus, for the k_1 and k_2 steps

$$k_1'A[\text{composite 1}] = k_1W[\text{composite 1}] \quad (21)$$

and

$$k_2'C[\text{composite 2}] = k_2Y[\text{composite 2}] \quad (22)$$

The rate for the proton-dependent model is on the right of the equal sign, and the rate for the proton-independent model is on the left of the equal sign. The primes identify the apparent rate constants at particular values of pH_o and pH_i; A is the fraction of composite 1 bound to ACh, and C is the fraction of composite 2 not bound to ACh. By canceling the composite concentrations, dividing eq 21 by eq 22, and substituting 100 for the ratio of k_1'/k_2', we obtain

$$k_1/k_2 \approx 100AY/(CW) \quad (23)$$

A and C include terms for the different protonation states of the transporter. Thus,

$$A = (1 + H_i\mathrm{r}1^{-1})/[1 + H_i\mathrm{r}1^{-1} + \mathrm{ACh_o r}^{-1} + H_o\mathrm{r}2/\mathrm{ACh_o r} + (\mathrm{ACh_o r} \times H_i\mathrm{r}1)^{-1} + H_o\mathrm{r}2/(\mathrm{ACh_o r} \times H_i\mathrm{r}1)] \quad (24)$$

which is the same as

$$A = W(1 + H_i\mathrm{r}1^{-1}) \quad (25)$$

and

$$C = (1 + H_i\mathrm{r}2^{-1} + H_o\mathrm{r}1 + H_o\mathrm{r}1/H_i\mathrm{r}2)/(1 + H_i\mathrm{r}2^{-1} + H_o\mathrm{r}1 + H_o\mathrm{r}1/H_i\mathrm{r}2 + \mathrm{ACh_i r}/H_i\mathrm{r}2 + H_o\mathrm{r}1 \times \mathrm{ACh_i r}/H_i\mathrm{r}2) \quad (26)$$

which is the same as

$$C = Y(1 + H_i\mathrm{r}2^{-1} + H_o\mathrm{r}1 + H_o\mathrm{r}1/H_i\mathrm{r}2) \quad (27)$$

By substituting eqs 25 and 27 into eq 23, we see that

$$k_1/k_2 \approx 100(1 + H_i\mathrm{r}1^{-1})/(1 + H_i\mathrm{r}2^{-1} + H_o\mathrm{r}1 + H_o\mathrm{r}1/H_i\mathrm{r}2) \quad (28)$$

Because $H_i\mathrm{r}2 \gg 1$ and $H_o\mathrm{r}1 \ll 1$ (see Results),

$$k_1/k_2 \approx 100(1 + H_i\mathrm{r}1)/H_i\mathrm{r}1 \quad (29)$$

In contrast to the time-dependent decrease in $H_i\mathrm{r}1$ following an external pH jump, $H_i\mathrm{r}1$ in eq 29 is a constant that depends on pK_{a1} and the pH_i of synaptic vesicles engaging in active transport of ACh driven by ATP. The true ratio of k_1/k_2 is larger than the apparent ratio determined by Bahr et al. (*5*) because site 1 is not fully protonated in ATP-driven transport. Thus, for example, if $pK_{a1} = 4.7$ and $pH_i = 5.3$ at steady state during ATP-driven transport, $H_i\mathrm{r}1 = 0.25$ and $k_1 = 500k_2$. In the single-proton model in which protonation is not necessary for the k_1-k_3 reorientation step, the apparent ratio of k_1/k_2 determined by Bahr et al. (*5*) is essentially equal to the true ratio.

ACKNOWLEDGMENT

We thank Ricardo Garcia and Barry Sanchez for preparation of synaptic vesicles and Dr. Edward D. Clarkson, III, for the gift of [^{3}H]analogue 16/17. We also thank Professor William Palke and Mr. Ezat Hosseini for help with the regression program and Professor David Hinkley with help on statistical analysis.

SUPPORTING INFORMATION AVAILABLE

Scientist computer programs for the one-proton and two-proton models along with extensive statistical measures of the goodness of fit and tables of the observed and calculated data for both models (46 pages). Ordering information is given on any current masthead page.

REFERENCES

1. Parsons, S. M., Prior, C., and Marshall, I. G. (1993) *Int. Rev. Neurobiol. 35*, 279−390.
2. Anderson, D. C., King, S. C., and Parsons, S. M. (1982) *Biochemistry 21*, 3037−3043.
3. Whittaker, V. P. (1988) *Handb. Exp. Pharmacol. 86*, 3−22.
4. Anderson, D. C., King, S. C., and Parsons, S. M. (1983) *Mol. Pharmacol. 24*, 48−54.
5. Bahr, B. A., Clarkson, E. D., Rogers, G. A., Noremberg, K., and Parsons, S. M. (1992) *Biochemistry 31*, 5752−5762.
6. Nguyen, M. L., and Parsons, S. M. (1995) *J. Neurochem. 64*, 1137−1142.
7. Gracz, L. M., and Parsons, S. M. (1996) *Biochim. Biophys. Acta 1292*, 293−302.
8. Bradford, M. M. (1976) *Anal. Biochem. 72*, 248−254.
9. Hendee, W. R. (1973) *Radioactive Isotopes in Biological Research*, p 215, Wiley, New York.
10. Noremberg, K., and Parsons, S. M. (1989) *J. Neurochem. 52*, 913−920.
11. Clarkson, E. D., Rogers, G. A., and Parsons, S. M. (1992) *J. Neurochem. 59*, 695−700.
12. Schuldiner, S. (1994) *J. Neurochem. 62*, 2067−2078.
13. Usdin, T. B., Eiden, L. E., Bonner, T. I., and Erickson, J. D. (1995) *Trends Neurosci. 18*, 218−224.

14. Erickson, J. D., Weihe, E., Schafer, M. K., Neale, E., Williamson, L., Bonner, T. I., Tao-Cheng, J. H., and Eiden, L. E. (1996) *Prog. Brain Res. 109*, 69−82.
15. Johnson, R. G., Jr. (1987) *Ann. N. Y. Acad. Sci. 493*, 162−177.
16. Varoqui, H., Diebler, M. F., Meunier, F. M., Rand, J. B., Usdin, T. B., Bonner, T. I., Eiden, L. E., and Erickson, J. D. (1994*) FEBS Lett. 342*, 97−102.
17. Song, H., Ming, G., Fon, E., Bellocchio, E., Edwards, R. H., and Poo, M. (1997) *Neuron 18*, 815−826.
18. Koslov, M. M., and Markin, V. S. (1984) *J. Theor. Biol. 109*, 17−39.
19. Varoqui, H., and Erickson, J. D. (1996) *J. Biol. Chem. 271*, 27229−27232.
20. Gracz, L. M., Wang, W.-C., and Parsons, S. M. (1988) *Biochemistry 27*, 5268−5274.
21. Barbosa, J., Jr., Clarizia, A. D., Gomez, M. V., Romano-Silva, M. A., Prado, V. F., and Prado, M. A. M. (1997) *J. Neurochem. 69*, 2608−2611.
22. Clarizia, A. D., Romano-Silva, M. A., Prado, V. F., Gomez, M. V., and Prado, M. A. M. (1998) *Neurosci. Lett. 244*, 115−117.
23. Van der Kloot, W. (1991) *Prog. Neurobiol. 36*, 93−130.
24. Van der Kloot, W., Benjamin, W. B., and Balezina, O. P. (1998) *J. Physiol. 507*, 689−695.
25. Betz, W. J., and Wu, L. G. (1995) *Curr. Biol. 5*, 1098−1101.
26. Henkel, A. W., and Betz, W. J. (1995) *J. Neurosci. 15*, 8246−8258.
27. Bonzelius, F., and Zimmermann, H. (1990) *J. Neurochem. 55*, 1266−1273.
28. MacIntosh, F. C., and Collier, B. (1976) *Handb. Exp. Pharmacol. 42*, 99−228.
29. Katz, B., and Miledi, R. (1981) *Proc. R. Soc. London, Ser. B 212*, 131−137.
30. Hille, B. (1984) *Ionic Channels of Excitable Membranes*, p 223, Sinauer Associates, Inc., Sunderland, MA.
31. Cha, S. (1968) *J. Biol. Chem. 243*, 820−825.

BI9802263